

Multifunctional PdAg@MIL-101 for One-Pot Cascade Reactions: Combination of Host–Guest Cooperation and Bimetallic Synergy in Catalysis

Yu-Zhen Chen,[†] Yu-Xiao Zhou,[†] Hengwei Wang,[†] Junling Lu,[†] Takeyuki Uchida,[‡] Qiang Xu,*^{*,‡} Shu-Hong Yu,[†] and Hai-Long Jiang^{*,†}

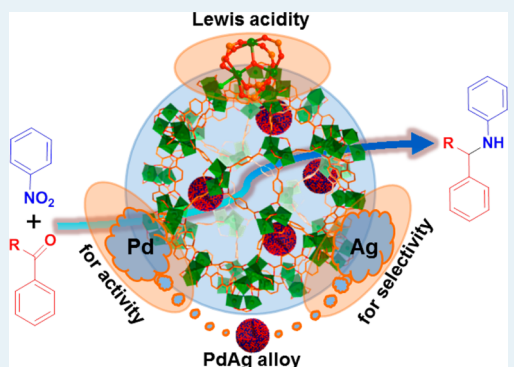
[†]Hefei National Laboratory for Physical Sciences at the Microscale, Key Laboratory of Soft Matter Chemistry, Chinese Academy of Sciences, Collaborative Innovation Center of Suzhou Nano Science and Technology, School of Chemistry and Materials Science, University of Science and Technology of China, Hefei, Anhui 230026, People's Republic of China

[‡]National Institute of Advanced Industrial Science and Technology (AIST), Ikeda, Osaka 563-8577, Japan

Supporting Information

ABSTRACT: Metal nanoparticles (NPs) stabilized by metal–organic frameworks (MOFs) are very promising for catalysis, while reports on their cooperative catalysis for a cascade reaction have been very rare. In this work, Pd NPs incorporated into a MOF, MIL-101, have jointly completed a tandem reaction on the basis of MOF Lewis acidity and Pd NPs. Subsequently, ultrafine PdAg alloy NPs (~ 1.5 nm) have been encapsulated into MIL-101. The obtained multifunctional PdAg@MIL-101 exhibits good catalytic activity and selectivity in cascade reactions under mild conditions, on the basis of the combination of host–guest cooperation and bimetallic synergy, where MIL-101 affords Lewis acidity and Pd offers hydrogenation activity while Ag greatly improves selectivity to the target product. As far as we know, this is the first work on bimetallic NP@MOFs as multifunctional catalysts with multiple active sites (MOF acidity and bimetallic species) that exert respective functions and cooperatively catalyze a one-pot cascade reaction.

KEYWORDS: metal–organic framework, heterogeneous catalysis, bimetallic nanoparticles, multifunctional catalyst, cascade reaction



1. INTRODUCTION

In modern synthetic chemistry, multistep reactions are often required to produce fine chemicals and final products. For multistep reactions, it is highly desired to obtain targeted products with high yield and selectivity in a simplified “one-pot” form over a multifunctional catalyst, which avoids time-consuming and tedious intermediate purification/separation processes and thus significantly reduces energy consumption and the cost of the final products.¹ Chemicals bearing a nitro group are versatile, are readily available by nitration, and are of particular interest as reactants or building blocks for multistep organic reactions. For example, nitroarenes can be hydrogenated to anilines, while further alkylation, reductive alkylation, or hydroamination transformation affords their value-added derivatives, including heterocyclic compounds.²

On the other hand, metal–organic frameworks (MOFs) have attracted great interest in the last two decades due to their modular assembly, high surface area, tunability, and tailorability as well as potential applications such as gas storage and separation, catalysis, sensing, drug delivery, proton conductivity, etc.^{3–7} In particular, MOFs have been widely reported as heterogeneous catalysts, mostly on the basis of the Lewis acid sites offered by unsaturated metal centers.⁸ Furthermore, the cages or channels with tunable sizes in MOFs allow them to

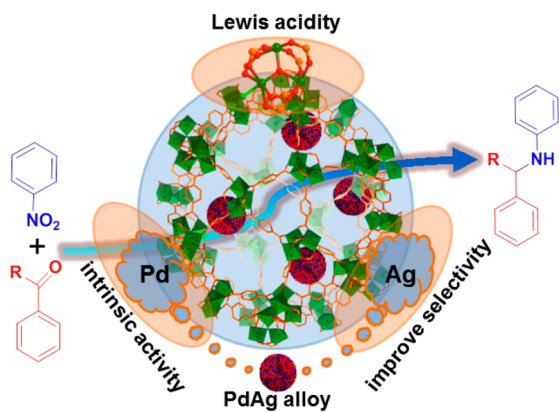
host or support metal nanoparticles (NPs) for catalysis over a broader scope; the crystalline porous structure of MOFs is expected to limit the migration and aggregation of metal NPs. In the past five years, there have been intensive studies on monometallic NP@MOFs,^{9,10} in which control of the location of metal NPs inside MOF cages/channels with tiny sizes remains very challenging. In addition, most of the previous work about the catalytic functions of metal NPs@MOF was based on metal NPs as the only active site. The nanocomposites designed for MOF–metal NP bifunctional (acid/base–metal) cooperative catalysis remain a largely unexplored field with very limited reports.¹⁰ Recently, we and others have reported several bimetallic NP@MOF examples which exhibit catalytic activity superior to that of their monometallic counterparts, ascribed to the modification of the electronic structures.¹¹ However, as far as we know, multifunctional catalysis over bimetallic NPs@MOF with three active sites (acid/base–metal A–metal B), which takes advantage of not only the catalytic synergy of bimetallic NPs but also the catalytic activity of the MOF itself, has never been reported.

Received: December 5, 2014

Revised: February 8, 2015

In this work, we have synthesized monometallic and bimetallic NP@MOF catalysts with tiny metal NPs inside MOF cages well-controlled via a double-solvent approach (DSA). The obtained PdAg alloy NPs show the smallest sizes among all bimetallic NPs stabilized by MOFs reported to date.¹¹ The Pd@MOF cooperatively catalyzes a tandem reaction on the basis of both MOF Lewis acidity and Pd NPs. Strikingly, the bimetallic PdAg@MOF bearing three active sites (Lewis acid–Pd–Ag) as a multifunctional catalyst has successfully realized one-pot multistep cascade reaction for the synthesis of secondary arylamines, by not only perfect cooperation between the MOF host and the metal NP guest but also synergistic catalysis between bimetallic Pd and Ag species (Scheme 1), in which the MOF affords Lewis acid sites,

Scheme 1. Schematic Illustration Showing the Multistep Reaction over PdAg@MIL-101 Involving Lewis Acid and Pd/Ag Sites



Pd offers hydrogenation activity, and Ag greatly improves selectivity toward the desired product. To the best of our knowledge, this is the first work that demonstrates an MOF host and the two species in bimetallic NP guest to functionalize like “three legs of a tripod” in catalysis and cooperatively boost one-pot multistep cascade reactions.

2. EXPERIMENTAL SECTION

2.1. Materials and Instrumentation. All chemicals were obtained from commercial sources and used without further purification. Powder X-ray diffraction patterns (XRD) were obtained on a Holland X’Pert PRO fixed anode X-ray diffractometer equipped with graphite-monochromated Cu K α radiation ($\lambda = 1.54178 \text{ \AA}$). The UV-vis absorption spectra were recorded on a UV-vis spectrophotometer (TU-1810, Beijing Pgeneral, People’s Republic of China) in the wavelength range of 200–800 nm. The surface acidity of the catalyst was measured by ammonia temperature-programmed desorption (NH₃-TPD); the profile was recorded using a gas chromatograph (TECHTEMP GC 7890II) with a TCD detector. The contents of Pd and Ag in the nanocomposite samples were quantified by an Optima 7300 DV inductively coupled plasma atomic emission spectrometer (ICP-AES). The size, morphology, and microstructure of Pd@MIL-101 and PdAg@MIL-101 were investigated by using transmission electron microscopy (TEM) and high-angle annular dark-field scanning transmission electron microscopy (HAADF-STEM) on JEOL-2010 and JEOL-2100F instruments with an electron acceleration energy of 200 kV. To verify whether NPs are really inside the MOF, a

series of HAADF-STEM images was taken for tilted samples with angle steps of 5° using a Tecnai G2 F20 transmission electron microscope operated at 200 kV. The nitrogen sorption isotherms were measured by using automatic volumetric adsorption equipment (Micrometrics ASAP 2020). Prior to nitrogen adsorption/desorption measurements, MIL-101 and its nanocomposite samples were evacuated at 160 °C for 12 h. The X-ray photoelectron spectroscopy (XPS) measurements were performed by using an ESCALAB 250 high-performance electron spectrometer using monochromated Al K α radiation ($h\nu = 1486.7 \text{ eV}$) as the excitation source. ¹H NMR was recorded on a Bruker AC-400 FT spectrometer (400 MHz) using TMS as internal reference. The catalytic reaction products were analyzed and identified by gas chromatography (GC, Shimadzu 2010 Plus with a 0.25 mm × 30 m Rtx-5 capillary column); GC-MS samples were recorded on a Shimadzu QP-5050 GC-MS system. The DRIFT spectra of CO adsorption were obtained on a Nicolet iS10 spectrometer with an MCT detector and a low-temperature reaction chamber (Harrick). Before DRIFT characterization, samples were given complete activation treatment. After pretreatment, an applicable amount of sample powder was loaded into the IR reflectance cell and purged by flowing helium (20 mL min⁻¹) for 120 min at 423 K under vacuum to remove the adsorbed water, and then the cell was cooled to 173 K with liquid nitrogen. CO adsorption was carried out by generally introducing 10% CO/He (5 mL min⁻¹) to the IR reflectance cell for almost 20 min.

2.2. Preparation of Samples. **2.2.1. Preparation of MIL-101.** MIL-101 was synthesized according to a previous report with modifications.¹² Typically, a mixture of terephthalic acid (332 mg, 2.0 mmol) with Cr(NO₃)₃·9H₂O (800 mg, 2.0 mmol) in the presence of aqueous HF (0.4 mL, 2.0 mmol) and deionized water (9.5 mL) was reacted at 200 °C for 8 h. The as-synthesized MIL-101 was refluxed in water, ethanol, and NH₄F solutions, respectively, for over 12 h, washed with hot water to eliminate the unreacted terephthalic acid trapped in the giant pores, and then finally dried overnight at 160 °C under vacuum for further use.

2.2.2. Preparation of Pd@MIL-101, Ag@MIL-101, and PdAg@MIL-101 via a Double-Solvent Approach (DSA). Typically, 200 mg of activated MIL-101 was suspended in 40 mL of a hydrophobic solvent of dry *n*-hexane, and the mixture was sonicated for around 20 min until it became homogeneous. After the mixture was stirred for a certain time, 0.30 mL of hydrophilic aqueous Pd(NO₃)₂·2H₂O and/or AgNO₃ solution with the desired concentrations was added dropwise with a syringe pump over a period of 20 min with constant vigorous stirring. Subsequently, the resultant solution was continuously stirred for 3 h. The harvested sample was further dried followed by treating in a stream of 20% H₂/Ar (40 mL min⁻¹) at 200 °C for 4 h to yield Pd@MIL-101, Ag@MIL-101, and PdAg@MIL-101. The Pd²⁺/(Pd²⁺ + Ag⁺) molar ratios were varied (0, 0.5, 0.67, 0.75, and 1.00) to optimize the activity of the resultant catalysts, while the molar amount of Pd²⁺ + Ag⁺ was fixed to be 0.017 mmol for 200 mg of the MIL-101 host matrix.

2.2.3. Preparation of Pd₂Ag₁MIL-101 via an Incipient Wetness Impregnation Method. Typically, 200 mg of activated MIL-101 was dispersed in 20 mL of water and the mixture was subject to ultrasonication for 20 min at room temperature. An aqueous solution containing 0.012 mmol of Pd(NO₃)₂·2H₂O and 0.006 mmol of AgNO₃ was added dropwise to the above solution under vigorous agitation for

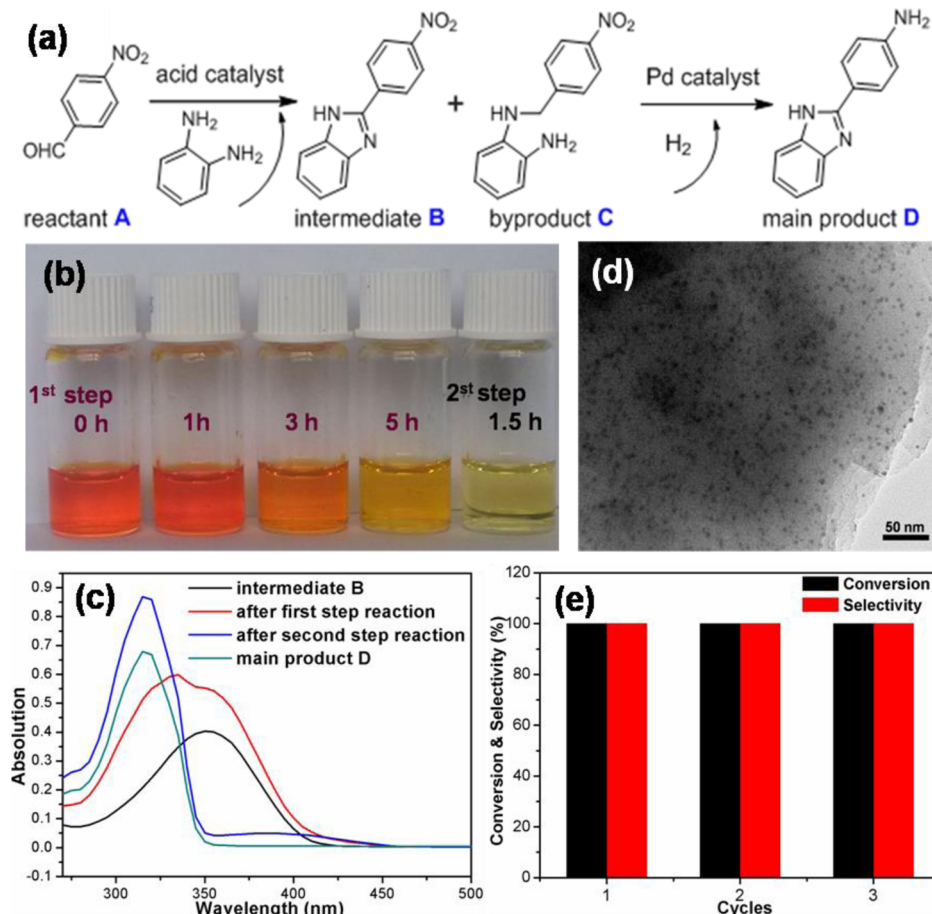


Figure 1. (a) Illustration of the two-step tandem synthesis of 2-(4-aminophenyl)-1*H*-benzimidazole (**D**) involving a Lewis acid based catalytic process and subsequent Pd based hydrogenation. (b) Solution color evolution during the reaction process. (c) UV–vis spectra tracking the catalytic reaction progress. The intermediate **B** and product **D** are pure substances obtained by column chromatographic separation. (d) Representative TEM image of Pd@MIL-101 catalyst. (e) Recycling performance for the conversion of **A** and selectivity to the target **D** after the two-step reaction over Pd@MIL-101.

about 30 min and was then magnetically agitated at room temperature for 24 h. The impregnated sample was washed with water until the filtrate became colorless to give Pd²⁺Ag⁺/MIL-101, followed by further drying at 50 °C for 12 h and treating under a stream of 20% H₂/Ar at 200 °C for 4 h to yield Pd₂Ag₁/MIL-101.

2.2.4. Preparation of Pd/Al₂O₃. A Pd(NO₃)₂·2H₂O (0.009 mmol) aqueous solution of an appropriate volume was slowly added dropwise to 100 mg of Al₂O₃ with vigorous agitation. The slurry was stirred at room temperature for 30 min and then dried at 50 °C for 12 h under vacuum. Finally, the sample was reduced at 200 °C for 4 h with 40 mL/min 20% H₂/Ar to give Pd/Al₂O₃.

2.3. Catalytic Activity Evaluation. **2.3.1. Catalytic Performance of Pd@MIL-101 and Other Catalysts for the Two-Step Tandem Reaction.** A 40 mg portion of dried Pd@MIL-101 was dispersed in 5 mL of methanol containing 0.5 mmol of 4-nitrobenzaldehyde and 0.6 mmol of 1,2-phenylenediamine, and the mixture was sonicated to be homogeneous. Then the resultant mixture was stirred at 80 °C in an air atmosphere for 5 h and then transferred into a 10 mL Teflon-lined pressure vessel without any separation or extraction. The vessel was then purged with H₂ ten times and pressurized with H₂ to 2 bar for the reaction at room temperature (25 °C) for 8 h. After the reaction, the catalyst was separated by centrifugation, thoroughly washed with ethanol, and then reutilized as catalyst in subsequent runs under identical reaction conditions. The yield of the product was analyzed by GC with an internal standard (dodecane). For comparison, 20 mg of Pd₂Ag₁/MIL-101, 20 mg of Pd/Al₂O₃, 20 mg of MIL-101, a physical mixture of Ag@MIL-101 and Pd@MIL-101 (with the same contents of

centrifugation, thoroughly washed with methanol, and then reutilized as the catalyst in subsequent runs under identical reaction conditions. The yield of the product was analyzed by GC. For comparison, 40 mg of MIL-101, 4 mg of commercial 10% Pd/C, or no catalyst was used for the reaction while all other reaction parameters and processes were kept the same.

2.3.2. Catalytic Performance of PdAg@MIL-101 and Other Catalysts for the Multistep Cascade Reaction. The catalytic reaction was performed in a 10 mL Teflon-lined stainless steel autoclave equipped with a pressure gauge and a magnetic stirrer. A 20 mg portion of dried PdAg@MIL-101 or Pd@MIL-101 catalyst was dispersed in 4 mL of ethanol containing 1 mmol of nitrobenzene and 1 mmol of benzaldehyde or acetophenone, and the mixture was sonicated to be homogeneous. The vessel was then purged with H₂ 10 times and pressurized with H₂ to 2 bar for the reaction. The reaction was conducted at room temperature (25 °C) and 110 °C for benzaldehyde and acetophenone, respectively, as substrates. After the reaction, the catalyst was separated by centrifugation, thoroughly washed with ethanol, and then reutilized as catalyst in subsequent runs under identical reaction conditions. The yield of the product was analyzed by GC with an internal standard (dodecane). For comparison, 20 mg of Pd₂Ag₁/MIL-101, 20 mg of Pd/Al₂O₃, 20 mg of MIL-101, a physical mixture of Ag@MIL-101 and Pd@MIL-101 (with the same contents of

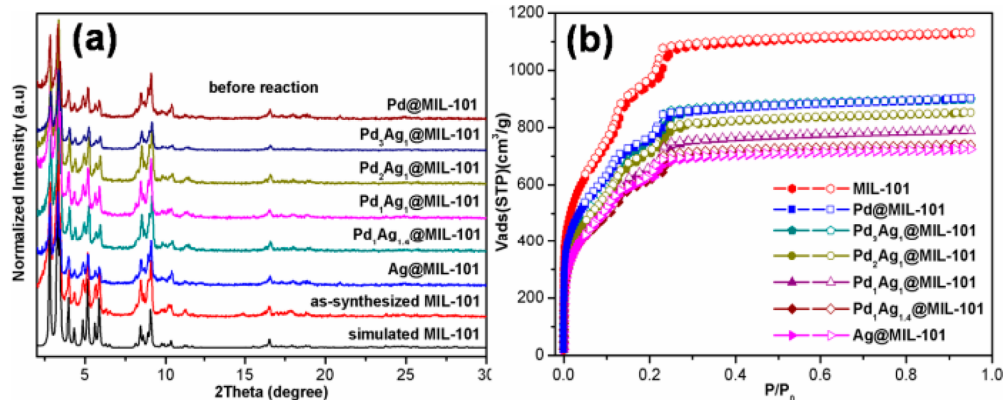


Figure 2. (a) Powder XRD profiles and (b) N₂ sorption isotherms at 77 K of as-synthesized MIL-101 and PdAg@MIL-101 catalysts before reaction. Filled and open symbols represent adsorption and desorption branches, respectively.

Pd and Ag as those in Pd₂Ag₁@MIL-101), 2 mg of commercial 10% Pd/C, or no catalyst was used for the reaction while all other reaction parameters and processes were kept the same.

3. RESULTS AND DISCUSSION

The MIL-101 framework, Cr₃X(H₂O)₂O(BDC)₃·nH₂O (BDC = benzene-1,4-dicarboxylate, X = F, OH, n ≈ 25),¹² one of the representative MOFs, was employed as a host. MIL-101 features a three-dimensional (3D) network with two types of giant cages with diameters of 2.9 and 3.4 nm and high physicochemical stability as well as a large surface area (BET, over 3600 m²/g), very suitable for encapsulating tiny metal NPs and hosting catalytic reactions. Moreover, MIL-101 can be activated upon heating to afford exposed Cr(III) centers serving as Lewis acid sites for catalysis.

To prevent the formation of metal NPs on the external surface of MOF and avoid their aggregation, a DSA synthetic approach was adopted to rationally introduce Pd or PdAg NPs to afford Pd@MIL-101 and PdAg@MIL-101, respectively (see the Experimental Section).^{11e,f} Given the huge cages with hydrophilic environments in MIL-101, the quantitative metal precursor aqueous solution should be fully incorporated into the MOF pores on the basis of capillary force and hydrophilic interactions during this process. The resultant metal precursors @MIL-101 were further reduced by H₂ to generate tiny metal NPs confined in MIL-101.

No diffraction peak in powder X-ray diffraction (PXRD) was detected for Pd NPs in Pd@MIL-101, revealing that Pd NPs could be small (Figure S1 in the Supporting Information). This assumption is consistent with the results of transmission electron microscopy (TEM) (Figure 1d), which shows that the Pd NPs in 1 wt % Pd@MIL-101 are highly dispersed with mean diameters of 2.5 ± 0.3 nm (Figure S2c in the Supporting Information). It is reasonably considered that Pd NPs with sizes smaller than the diameters of MOF cages have been successfully confined inside the MOF as predesigned.

To demonstrate that Pd@MIL-101 can be used for tandem catalysis, a reaction route involving acid catalysis and catalytic hydrogenation steps was chosen for the synthesis of 2-(4-aminophenyl)-1*H*-benzimidazole (**D**) (Figure 1a), which is biologically active and is a key intermediate in the synthesis of benzimidazole derivatives for antiviral, antilulcer, and anticancer ends.¹³ Figure 1b shows the solution color evolution for the Pd@MIL-101 catalyzed reaction, recording the progress after 0, 1, 3, and 5 h of the first step of acid catalysis and after 1.5 h of

the second step of catalytic hydrogenation, respectively. The solution color becomes gradually more faint as the time increases in the cascade reaction. In addition, UV-vis spectra were used to track the catalytic reaction progress of the two-step tandem synthesis of **D** based on Pd@MIL-101 catalyst. The peak has an evident blue shift during the reaction (Figure 1c). In situ FT-IR spectra of CO adsorption for both MIL-101 and Pd@MIL-101 at 158 K showing a band at ~2190 cm⁻¹ could be ascribed to CO coordinated at open Cr³⁺ Lewis acid sites (Figure S3 in the Supporting Information).⁹ⁱ The NH₃ temperature-programmed desorption (TPD) for MIL-101 and Pd@MIL-101 shows a broad peak in the range of 186–420 °C, which could be assigned to NH₃ adsorption on the open Cr³⁺ Lewis acid sites at <300 °C and partial decomposition of MIL-101 at higher temperature (Figure S4 in the Supporting Information), further validating its Lewis acidity. The intermediate 2-(4-aminophenyl)-1*H*-benzimidazole (**B**), the intermediate byproduct **C**, and the target product **D** were identified by GC-MS spectrometry and ¹H NMR, respectively (Figures S5 and S6 in the Supporting Information). Almost 100% conversion of the reactant 4-nitrobenzaldehyde in the acid catalysis step and a >99% yield of **D** were obtained over Pd@MIL-101 catalyst bearing dual active sites (Figure 1a). In contrast, previous yolk-shell Pd@mesoporous aluminosilica and nonrecyclable catalysts gave lower yields (~90% and ~80%, respectively), and even the latter requires time-consuming procedures.¹⁴ In the control experiment, only 30% reactant was converted to **C** in the absence of catalyst. When commercial Pd/C catalyst was used, about 50% of the reactants was converted to **C** in the first step due to the lack of acidity, and therefore the nitro group in both the residual reactant and **C** was coreduced to corresponding amino group in the second step. The reaction was terminated after the first step and produced only **B** over MIL-101 catalyst without Pd NPs. The reusability tests for Pd@MIL-101 catalyst have clearly indicated that the excellent catalytic activity and selectivity remain high over three runs (Figure 1e). TEM observations for Pd@MIL-101 have also shown that the sizes of Pd NPs are well retained even after three runs (Figure S2 in the Supporting Information). All of these results suggest that both the synergistic effect between Lewis acidity and Pd NPs and the confinement effect of MIL-101 play important roles in the catalytic performance of Pd@MIL-101.

Encouraged by the extraordinary catalytic activity, selectivity, and recyclability as well as the great size restriction of Pd NPs in bifunctional Pd@MIL-101 catalyst in the above tandem

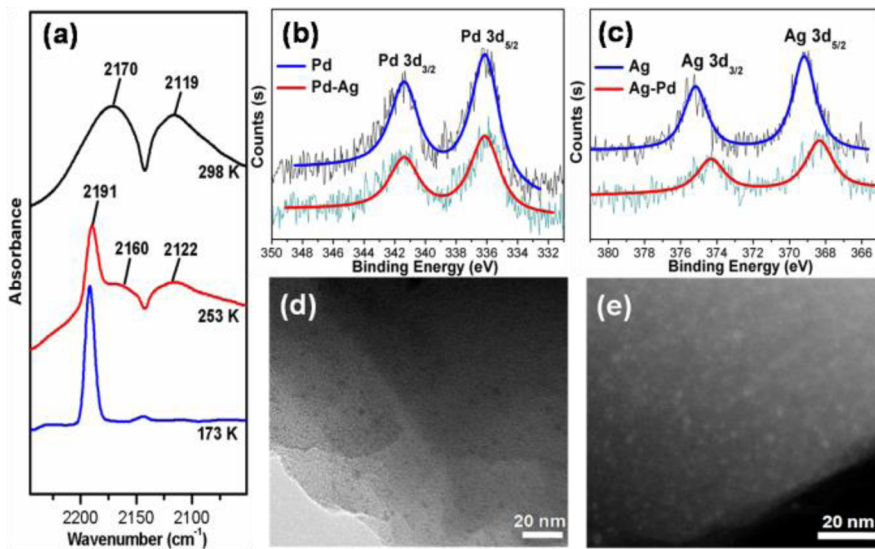


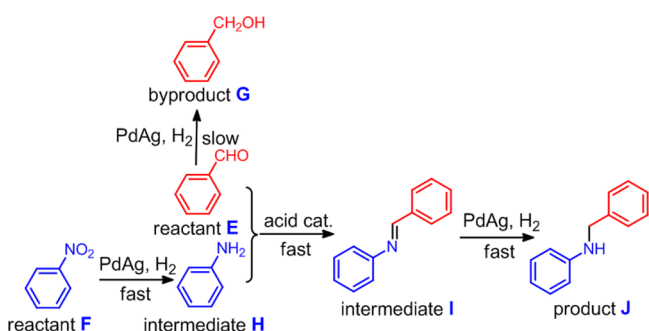
Figure 3. (a) In situ FT-IR spectra of CO adsorbed on Pd₂Ag₁@MIL-101 at different temperatures. XPS spectra of (b) Pd 3d and (c) Ag 3d for Pd@MIL-101, Pd₂Ag₁@MIL-101, and Ag@MIL-101. (d) TEM and (e) HAADF-STEM images showing the ultrafine PdAg NPs in Pd₂Ag₁@MIL-101.

reaction, bimetallic PdAg@MIL-101 species with various Pd/Ag ratios have been synthesized via a similar DSA approach. Inductively coupled plasma atomic emission spectrometry (ICP-AES) has confirmed that the actual contents of Pd and Ag are close to the nominal values and the Pd/Ag ratios match the predetermined trend (Table S1 in the Supporting Information). The crystallinity of MIL-101 upon loading Pd/Ag species has been proven by PXRD results (Figure 2a and Figure S7 in the Supporting Information). The BET surface areas of as-synthesized MIL-101, Pd@MIL-101, Pd₃Ag₁@MIL-101, Pd₂Ag₁@MIL-101, Pd₁Ag₁@MIL-101, Pd₁Ag_{1.4}@MIL-101, and Ag@MIL-101 were 3660, 2784, 2826, 2696, 2465, 2499, and 2322 m²/g, respectively, implying that the cavities of the host framework are possibly occupied by highly dispersed metal NPs (Figure 2b). Similar to that of Pd@MIL-101, the in situ DRIFT IR spectrum of CO adsorbed on PdAg@MIL-101 at 173 K displays a strong peak at 2191 cm⁻¹ attributed to CO coordinated at open Cr³⁺ Lewis acid sites (Figure 3a). The peak significantly decreases with elevated temperature, while the bands at 2119 and 2170 cm⁻¹ assigned to CO physisorption or gaseous CO present gradually higher intensity with an increase in temperature to 253 and 298 K.¹⁵ The X-ray photoelectron spectroscopy (XPS) results show that both Pd and Ag are in the reduced states and the 3d peaks for Pd(0) and Ag(0) in Pd₂Ag₁@MIL-101 shift to lower binding energies by ~0.2 and ~0.8 eV, respectively (Figure 3b,c), in comparison to those in monometallic Pd@MIL-101 and Ag@MIL-101. Moreover, the 3d peaks for Ag(0) shift gradually to lower binding energies with decreasing contents of Ag, and the 3d_{5/2} peak of Pd(0) also gradually shifts to lower binding energies with decreasing contents of Pd in PdAg@MIL-101. Such observed shifts for both Pd 3d and Ag 3d may be attributed to the flow of electron density from Ag to Pd (gaining electrons from Ag), indicative of the presence of an interaction between Ag and Pd and the formation of PdAg alloy NPs (Figure S8 and Table S2 in the Supporting Information), in good agreement with previous reports.^{11d,g,16} The formation of PdAg alloy NPs is reasonable because the two soluble metal salts have close reduction potentials ($E^\circ_{\text{Pd}^{2+}/\text{Pd}} = +0.915 \text{ eV}$ vs SHE; $E^\circ_{\text{Ag}^+/\text{Ag}} = +0.80 \text{ eV}$ vs SHE). Upon heating under an H₂/Ar flow, both Pd²⁺ and Ag⁺ would be simultaneously reduced to afford PdAg alloys.

Unexpectedly, very tiny PdAg NPs with sizes of $1.5 \pm 0.3 \text{ nm}$ were formed on the basis of TEM and high-angle annular dark-field scanning transmission electron microscopy (HAADF-STEM) observations (Figure 3d,e and Figure S9 in the Supporting Information). In addition, a series of HAADF-STEM images was taken for tilted Pd₂Ag₁@MIL-101 with angle steps of 5° and the results clearly demonstrated that PdAg NPs were trapped inside MIL-101 (see videos in the Supporting Information), revealing the successful induction of Pd²⁺ and Ag⁺ into MOF cages via the DSA approach and the ideal confinement effect of MIL-101 for PdAg NPs. To our knowledge, this is the smallest size of bimetallic NPs that have been confined inside MOFs reported thus far.¹¹ It is proposed that Ag effectively reduces the aggregation of Pd NPs, thus resulting in the smaller PdAg NP sizes in comparison to those of Pd NPs in Pd@MIL-101. This is a very interesting while unusual finding that alloying allows even smaller particle sizes confined in a MOF under similar synthetic conditions.

The ultrafine PdAg NPs are expected to offer excellent performance in heterogeneous catalysis. The coexistence of Lewis acid sites in MIL-101 and bimetallic Pd and Ag species may render PdAg@MIL-101 a multifunctional catalyst that is suitable for multistep cascade reactions. Therefore, a one-pot multistep conversion of nitroarene to value-added secondary arylamine has been explored over PdAg@MIL-101. The overall three-step process involves nitroarene hydrogenation, reductive amination of aldehydes or ketones, and selective hydrogenation to secondary arylamine. The results of the reaction over different PdAg@MIL-101 catalysts, PdAg/MIL-101, Pd/Al₂O₃, a physical mixture of Pd@MIL-101 and Ag@MIL-101, or commercial Pd/C or in the absence of catalyst are shown in Table 1. The monometallic Pd@MIL-101 has high catalytic activity and rapidly completes the conversion with low selectivity of the main product (entry 1). Significantly, the alloying of Pd with Ag allows the catalyst to complete the conversion in a slightly longer time but affords higher selectivity to the desired product of secondary arylamine (entries 2–5). As the ratio of Ag/Pd increases, a clear trend of decreased activity with increased selectivity is observed. Evidently, Pd NPs have intrinsic hydrogenation activity while Ag greatly improves the selectivity of the target product. Given the Pd–Ag

Table 1. Synthesis of Secondary Arylamines through Hydrogenation of Nitrobenzene and Reductive Amination of Benzaldehyde^a



entry	catalyst	time (h)	conversn ^b (%)	selectivity ^b (%)		
				J	I	G
1	Pd@MIL-101	3	100	56	1	43
2	Pd ₃ Ag ₁ @MIL-101	6	100	77	0	23
3	Pd ₂ Ag ₁ @MIL-101	10	99	85	1	14
4	Pd ₁ Ag ₁ @MIL-101	28	99	90	3	7
5	Pd ₁ Ag _{1.4} @MIL-101	40	40	66	23	11
6	Ag@MIL-101					
7	Pd ₂ Ag ₁ @MIL-101	24	99	63	1	36
8	Pd/Al ₂ O ₃	3	67	53	20	27
9 ^c	Pd@MIL-101 + Ag@MIL-101	10	70	61	4	35
10	Pd/C	3	100	31	0	69
11	MIL-101					
12	no					

^aReaction conditions: substrates E (1.0 mmol) and F (1.0 mmol), 0.17 mol % catalyst (based on *n*(Pd+Ag)) in 4 mL of ethanol at room temperature, 0.2 MPa of H₂. ^bConversion of E and selectivity were analyzed by GC, and *n*-dodecane was used as the internal standard. ^cThe catalytic result was based on a physical mixture of Pd@MIL-101 and Ag@MIL-101, in which the contents of Pd and Ag are the same as those in Pd₂Ag₁@MIL-101.

interaction reflected by the XPS data (Figure S8 in the Supporting Information) and the electronic effect of Ag making the reaction proceed preferably toward the target product, it is proposed that the addition of Ag will slow down the reduction rate of benzaldehyde to generate alcohol and lead to higher conversion of benzaldehyde to secondary arylamine.¹⁷ As a result, higher selectivity to the desired product was obtained when increasing the ratio of Ag in PdAg alloy, while Ag contents that are too high will lead to sluggish reaction rates because Ag species are inactive for the conversion of nitroarene to aminoarene (entry 6). For comparison, Pd₂Ag₁/MIL-101 was prepared by incipient wetness impregnation, which exhibited only 63% selectivity to the target product after 24 h, possibly due to the lack of sufficient confinement effects for the PdAg NPs (entry 7). Similarly, the Pd/Al₂O₃ presented lower catalytic activity than Pd@MIL-101 and also quite low selectivity, although in the presence of Lewis acidity (entry 8). In addition, the lower catalytic activity and selectivity over a physical mixture of Pd@MIL-101 and Ag@MIL-101 in comparison to those of Pd₂Ag₁@MIL-101 indicated the possible formation of Pd–Ag bimetallic NPs in MIL-101 (entry 9). Commercial Pd/C has high activity similar to that of Pd@MIL-101 catalyst but even lower selectivity (30%), reflecting the critical role of acidity in the reaction between

nitrobenzene and benzaldehyde (entry 10). The reaction does not occur with MIL-101 or in the absence of catalyst (entries 11 and 12). The results perfectly demonstrate the significance of the triply synergistic effect of acidity and Pd and Ag species, with which the one-pot multistep reaction can be achieved with good activity and selectivity under very moderate conditions (25 °C, 0.2 MPa of H₂). To optimize the reaction parameters, both ethanol and toluene were employed as solvents, and the results show that the former is slightly better (Table 1 and Table S3 in the Supporting Information).

To understand the role of the Lewis acid sites in MIL-101 for the reaction, a control experiment was conducted with a pyridine probe. The reaction immediately stops upon the introduction of pyridine (100 μL) into the system when the reaction has proceeded for 7 h. In contrast, for the Pd/C-catalyzed system, the reaction has no influence when pyridine was introduced, revealing that pyridine is able to terminate the reaction by poisoning of the Lewis acid sites of MIL-101 while not by capping Pd or PdAg NPs (Figure 4). The phenomenon

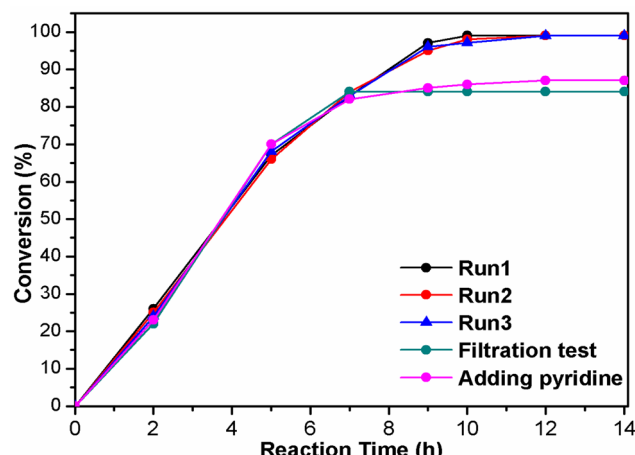


Figure 4. Recycling and filtration tests as well as the control experiment with introduction of pyridine during the reaction process over Pd₂Ag₁@MIL-101 catalyst.

can be readily explained with the poisoning of the Lewis acid sites by strong interactions with pyridine.^{5f} This result offers solid evidence to support the presence of Lewis acid active sites in MIL-101 and demonstrate its significant influence on the catalytic performance. In addition, the catalytic activity and selectivity over Pd₂Ag₁@MIL-101 are well preserved even after three cycles (Figure 4 and Figure S10 in the Supporting Information), suggesting its good recyclability and durability.

No significant loss of crystallinity and no identifiable peaks for metal NPs in the PXRD patterns occurs after three runs or in the presence of pyridine. The results reveal the retained integrity of the MIL-101 framework and the nonexistence of metal NP agglomeration (Figure S7 in the Supporting Information), which finds further evidence in TEM and HAADF-STEM images that PdAg NPs have well retained sizes after three cycles (Figure 5 and Figure S9 in the Supporting Information), demonstrating the great confinement effect of MIL-101 and structural stability of the catalyst.

On the basis of the above results, the Lewis acidity in both Pd@MIL-101 and PdAg@MIL-101 catalysts is supported by the following evidence. (1) Both CO FT-IR and NH₃-TPD spectra show the available unsaturated Cr(III) centers in MIL-101 and reveal the presence of Lewis acid sites, as

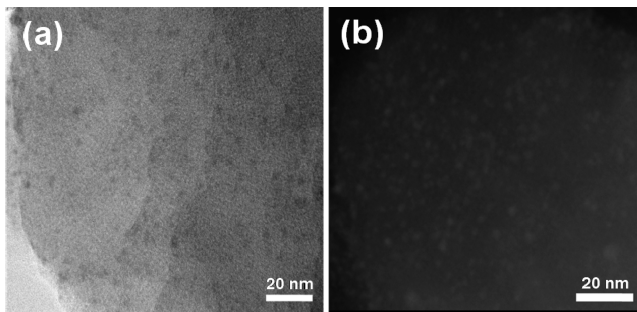


Figure 5. (a) TEM and (b) HAADF-STEM images for $\text{Pd}_2\text{Ag}_1@\text{MIL}-101$ catalyst after three runs of the reaction.

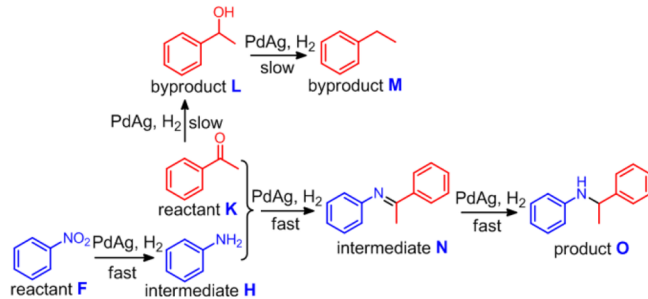
demonstrated in previous reports.^{8a,9i,10a} (2) For the first step in the tandem reaction, almost 100% conversion of the 4-nitrobenzaldehyde in the acid catalysis step and >99% yield of the desired product (**D**) were obtained over $\text{Pd}@\text{MIL}-101$ catalyst. However, for the commercial Pd/C catalyst, only about 50% yield was obtained. The results indicated the presence of Lewis acidity in $\text{Pd}@\text{MIL}-101$. (3) The second reaction between nitrobenzene and benzaldehyde presents good selectivity to the target product (**J**) with acidity-involved catalyst. In contrast, the benzaldehyde is prone to be reduced in preference to benzyl alcohol in the absence of acidity, although the reaction between aniline and benzaldehyde proceeds slightly, as supported by the fact that commercial Pd/C catalyst gives only 31% selectivity to target **J**. The comparison results among $\text{Pd}/\text{MIL}-101$, $\text{Pd}_2\text{Ag}_1/\text{MIL}-101$, and Pd/C catalysts reflect the critical role of the acidity in $\text{MIL}-101$ for the reaction. (4) Pyridine has been introduced into both reaction systems in the presence of $\text{Pd}_2\text{Ag}_1/\text{MIL}-101$ and Pd/C for comparison. The results clearly show that the pyridine as a Lewis base terminates the reaction toward the production of target **J** by poisoning of the Lewis acid sites of $\text{MIL}-101$ while not by capping Pd or PdAg NPs.

Given the great performance of $\text{Pd}_2\text{Ag}_1@\text{MIL}-101$ catalyst for the cascade nitroarene hydrogenation–reductive amination of aldehydes, and to further illustrate the Lewis acid role in the catalyst, the aldehyde has been replaced by the more inert acetophenone in the second reaction, and then the reaction requires higher acidity.^{2b} The commercial Pd/C catalyst gives 88% conversion after 60 h while the product was exclusively phenylethanol without even traces of the imine or secondary amine, due to the lack of required acidity. In sharp contrast, with strong Lewis acidity, the $\text{Pd}_2\text{Ag}_1@\text{MIL}-101$ catalyst effectively promotes the reaction to convert 65% acetophenone in 30 h with 71% selectivity toward the target secondary amine (Table 2). The much higher selectivity of the title catalyst toward the secondary amine with respect to Pd/C evidences the advantages of using $\text{MIL}-101$, which not only acts as a porous host for incorporating active PdAg NPs but also actively participates in the reaction with Lewis acid sites.

4. CONCLUSION

In summary, a MTN zeolite-type MOF, $\text{MIL}-101$, with large cages has been employed to confine Pd NPs with sizes of ~2.5 nm on the basis of a DSA encapsulation followed by H_2 reduction. The obtained $\text{Pd}@\text{MIL}-101$ behaves as a bifunctional catalyst and presents excellent performance in tandem catalysis, a reaction route involving acid catalysis and a catalytic hydrogenation process for the synthesis of 2-(4-aminophenyl)-

Table 2. Synthesis of Secondary Arylamines through Hydrogenation of Nitrobenzene and Reductive Amination of Acetophenone^a



catalyst	time (h)	conversn ^b (%)	selectivity ^b (%)		
			O	L	M
Pd/C	60	88	73	27	
$\text{Pd}_2\text{Ag}_1@\text{MIL}-101$	30	65	71	14	15

^aReaction conditions: substrates **K** (1.0 mmol), and **F** (1.0 mmol), 0.46 mol % catalyst (based on *n*(Pd+Ag)) in 4 mL of ethanol at 110 °C, 0.2 MPa of H_2 . ^bConversion of **E** and selectivity were analyzed by GC and GC-MS.

1*H*-benzimidazole. Following a similar approach, ultrafine PdAg alloy NPs (~1.5 nm) have been encapsulated into $\text{MIL}-101$ and the resultant multifunctional catalyst, for the first time, has fulfilled a one-pot multistep cascade conversion of nitroarene to secondary arylamine through the combination of host–guest cooperation and guest bimetallic synergy, in which MOF affords Lewis acid sites and Pd offers hydrogenation activity while Ag greatly improves selectivity toward the target secondary amine. The facile and rational preparation as well as excellent activity, selectivity, and recyclability of $\text{PdAg}@\text{MIL}-101$ in this work might open a new avenue to MOF-based multifunctional catalysts, which has great potential for broad applications in one-pot cascade reactions for the synthesis of organic chemicals in the future.

■ ASSOCIATED CONTENT

● Supporting Information

The following files are available free of charge on the ACS Publications website at DOI: 10.1021/cs501953d.

Experimental details, NH_3 -TPD profiles, FT-IR, GC-MS, and ^1H NMR spectra, TEM images, XRD patterns, and Tables S1–S3 (PDF)

HAADF-STEM images for tilted $\text{Pd}_2\text{Ag}_1@\text{MIL}-101$ (AVI)

HAADF-STEM images for tilted $\text{Pd}_2\text{Ag}_1@\text{MIL}-101$ (AVI)

■ AUTHOR INFORMATION

Corresponding Authors

*E-mail for Q.X.: q.xu@aist.go.jp.

*E-mail for H.-L.J.: jianglab@ustc.edu.cn.

Notes

The authors declare no competing financial interest.

■ ACKNOWLEDGMENTS

We gratefully thank the reviewers for their valuable suggestions. This work was supported by the NSFC (21371162 and 51301159), the 973 program (2014CB931803), the NSF of

Anhui Province (1408085MB23), the Research Fund for the Doctoral Program of Higher Education of China (20133402120020), the Recruitment Program of Global Youth Experts, and the Fundamental Research Funds for the Central Universities (WK2060190026).

■ REFERENCES

- (1) (a) Ajamian, A.; Gleason, J. L. *Angew. Chem., Int. Ed.* **2004**, *43*, 3754–3760. (b) Lee, J. M.; Na, Y.; Han, H.; Chang, S. *Chem. Soc. Rev.* **2004**, *33*, 302–312. (c) Barluenga, J.; Mendoza, A.; Rodríguez, F.; Fañanás, F. J. *Angew. Chem., Int. Ed.* **2008**, *47*, 7044–7047. (d) Climent, M. J.; Corma, A.; Iborra, S.; Sabater, M. J. *ACS Catal.* **2014**, *4*, 870–891.
- (2) (a) Blaser, H.-U.; Malan, C.; Pugin, B.; Spindler, F.; Steiner, H.; Studer, M. *Adv. Synth. Catal.* **2003**, *345*, 103–151. (b) Sreedhar, B.; Surendra Reddy, P.; Keerthi Devi, D. *J. Org. Chem.* **2009**, *74*, 8806–8809.
- (3) (a) Long, J. R.; Yaghi, O. M. *Chem. Soc. Rev.* **2009**, *38*, 1213–2114. (b) Zhou, H.-C.; Long, J. R.; Yaghi, O. M. *Chem. Rev.* **2012**, *112*, 673–674. (c) Furukawa, H.; Cordova, K. E.; O’Keeffe, M.; Yaghi, O. M. *Science* **2013**, *341*, 974–986. (d) Cook, T. R.; Zheng, Y.-R.; Stang, P. *J. Chem. Rev.* **2013**, *113*, 734–777. (e) Zhou, H.-C.; Kitagawa, S. *Chem. Soc. Rev.* **2014**, *43*, 5415–5418.
- (4) (a) Ma, S.; Zhou, H.-C. *Chem. Commun.* **2010**, *46*, 44–53. (b) Sumida, K.; Rogow, D. L.; Mason, J. A.; McDonald, T. M.; Bloch, E. D.; Herm, Z. R.; Bae, T.-H.; Long, J. R. *Chem. Rev.* **2012**, *112*, 724–781. (c) Suh, M. P.; Park, H. J.; Prasad, T. K.; Lim, D.-W. *Chem. Rev.* **2012**, *112*, 782–835. (d) Nugent, P.; Belmabkhout, Y.; Burd, S. D.; Cairns, A. J.; Luebke, R.; Forrest, K.; Pham, T.; Ma, S.; Space, B.; Wojtas, L.; Eddaoudi, M.; Zaworotko, M. J. *Nature* **2013**, *495*, 80–84. (e) Li, J.-R.; Sculley, J.; Zhou, H.-C. *Chem. Rev.* **2012**, *112*, 869–932. (f) He, Y.; Zhou, W.; Qian, G.; Chen, B. *Chem. Soc. Rev.* **2014**, *43*, 5657–5678. (g) Hu, Y.; Verdegaal, W. M.; Yu, S.-H.; Jiang, H.-L. *ChemSusChem* **2014**, *7*, 734–737.
- (5) (a) Seo, J. S.; Whang, D.; Lee, H.; Jun, S. I.; Oh, J.; Jeon, Y. J.; Kim, K. *Nature* **2000**, *404*, 982–986. (b) Farrusseng, D.; Aguado, S.; Pinel, C. *Angew. Chem., Int. Ed.* **2009**, *48*, 7502–7513. (c) Corma, A.; García, H.; Llabrés i Xamena, F. X. *Chem. Rev.* **2010**, *110*, 4606–4655. (d) Jiang, H.-L.; Xu, Q. *Chem. Commun.* **2011**, *47*, 3351–3370. (e) Gascon, J.; Corma, A.; Kapteijn, F.; Llabrés i Xamena, F. X. *ACS Catal.* **2014**, *4*, 361–378. (f) Dhakshinamoorthy, A.; Alvaro, M.; Garcia, H. *Chem. Eur. J.* **2010**, *16*, 8530–8536. (g) Zhang, T.; Lin, W. *Chem. Soc. Rev.* **2014**, *43*, 5982–5993. (h) Liu, J.; Chen, L.; Cui, H.; Zhang, J.; Zhang, L.; Su, C.-Y. *Chem. Soc. Rev.* **2014**, *43*, 6011–6061. (i) Fu, Y.; Sun, D.; Chen, Y.; Huang, R.; Ding, Z.; Fu, X.; Li, Z. *Angew. Chem., Int. Ed.* **2012**, *51*, 3364–3367. (j) Liu, Y.; Tang, Z. *Adv. Mater.* **2013**, *25*, 5819–5825.
- (6) (a) Chen, B.; Xiang, S.; Qian, G. *Acc. Chem. Res.* **2010**, *43*, 1115–1124. (b) Takashima, Y.; Martinez, V.; Furukawa, S.; Kondo, M.; Shimomura, S.; Uehara, H.; Nakahama, M.; Sugimoto, K.; Kitagawa, S. *Nat. Commun.* **2011**, *2*, 168. (c) Kreno, L. E.; Leong, K.; Farha, O. K.; Allendorf, M.; Van Duyne, R. P.; Hupp, J. T. *Chem. Rev.* **2012**, *112*, 1105–1125. (d) Lin, R.-B.; Li, F.; Liu, S.-Y.; Qi, X.-L.; Zhang, J.-P.; Chen, X.-M. *Angew. Chem., Int. Ed.* **2013**, *52*, 13429–13433. (e) Hu, Z.; Deibert, B. J.; Li, J. *Chem. Soc. Rev.* **2014**, *43*, 5815–5840. (f) Zhang, M.; Feng, G.; Song, Z.; Zhou, Y.-P.; Chao, H.-Y.; Yuan, D.; Tan, T. T. Y.; Guo, Z.; Hu, Z.; Tang, B. Z.; Liu, B.; Zhao, D. *J. Am. Chem. Soc.* **2014**, *136*, 7241–7244.
- (7) (a) Wang, Z.; Cohen, S. M. *Chem. Soc. Rev.* **2009**, *38*, 1315–1349. (b) An, J.; Geib, S. J.; Rosi, N. L. *J. Am. Chem. Soc.* **2009**, *131*, 8376–8377. (c) Horcajada, P.; Gref, R.; Baati, T.; Allan, P. K.; Maurin, G.; Couvreur, P.; Férey, G.; Morris, R. E.; Serre, C. *Chem. Rev.* **2012**, *112*, 1232–1268. (d) Ramaswamy, P.; Wong, N. E.; Shimizu, G. K. H. *Chem. Soc. Rev.* **2014**, *43*, 5913–5932. (e) Mallick, A.; Garai, B.; Díaz, D. D.; Banerjee, R. *Angew. Chem., Int. Ed.* **2013**, *52*, 13755–13759. (f) Kitagawa, H. *Nat. Chem.* **2009**, *1*, 689–690.
- (8) (a) Schlichte, K.; Kratzke, T.; Kaskel, S. *Microporous Mesoporous Mater.* **2004**, *73*, 81–88. (b) Horike, S.; Dincă, M.; Tamaki, K.; Long, J. R. *J. Am. Chem. Soc.* **2008**, *130*, 5854–5855. (c) Vermoortele, F.; Bueken, B.; Bars, G. L.; Voorde, B. V. d.; Vandichel, M.; Houthoofd, K.; Vimont, A.; Daturi, M.; Waroquier, M.; Speybroeck, V. V.; Kirschhock, C.; DeVos, D. E. *J. Am. Chem. Soc.* **2013**, *135*, 11465–11468.
- (9) (a) Hermes, S.; Schröter, M.-K.; Schmid, R.; Khodeir, L.; Muhler, M.; Tissler, A.; Fischer, R. W.; Fischer, R. A. *Angew. Chem., Int. Ed.* **2005**, *44*, 6237–6241. (b) Moon, H. R.; Kim, J. H.; Suh, M. P. *Angew. Chem., Int. Ed.* **2005**, *44*, 1261–1265. (c) Hwang, Y. K.; Hong, D. Y.; Chang, J. S.; Jhung, S. H.; Seo, Y. K.; Kim, J.; Vimont, A.; Daturi, M.; Serre, C.; Férey, G. *Angew. Chem., Int. Ed.* **2008**, *47*, 4144–4148. (d) Jiang, H.-L.; Liu, B.; Akita, T.; Haruta, M.; Sakurai, H.; Xu, Q. *J. Am. Chem. Soc.* **2009**, *131*, 11302–11303. (e) Houk, R. J. T.; Jacobs, B. W.; Gabaly, F. E.; Chang, N. N.; Talin, A. A.; Graham, D. D.; House, S. D.; Robertson, I. M.; Allendorf, M. D. *Nano Lett.* **2009**, *9*, 3413–3418. (f) Yuan, B.; Pan, Y.; Li, Y.; Yin, B.; Jiang, H. *Angew. Chem., Int. Ed.* **2010**, *49*, 4054–4058. (g) Lu, G.; Li, S.; Guo, Z.; Farha, O. K.; Hauser, B. G.; Qi, X.; Wang, Y.; Wang, X.; Han, S.; Liu, X.; DuChene, J. S.; Zhang, H.; Zhang, Q.; Chen, X.; Ma, J.; Loo, S. C. J.; Wei, W. D.; Yang, Y.; Hupp, T. J.; Huo, F. *Nat. Chem.* **2012**, *4*, 310–316. (h) Kuo, C. H.; Tang, Y.; Chou, L. Y.; Sneed, B. T.; Brodsky, C. N.; Zhao, Z. P.; Tsung, C.-K. *J. Am. Chem. Soc.* **2012**, *134*, 14345–14348. (i) Khajavi, H.; Stil, H. A.; Kuipers, H. P. C. E.; Gascon, J.; Kapteijn, F. *ACS Catal.* **2013**, *3*, 2617–2626. (j) He, L.; Liu, Y.; Liu, J.; Xiong, Y.; Zheng, J.; Liu, Y.; Tang, Z. *Angew. Chem., Int. Ed.* **2013**, *52*, 3741–3745. (k) Zhang, Z.; Chen, Y.; Xu, X.; Zhang, J.; Xiang, G.; He, W.; Wang, X. *Angew. Chem., Int. Ed.* **2014**, *53*, 429–433. (l) Na, K.; Choi, K. M.; Yaghi, O. M.; Somorjai, G. A. *Nano Lett.* **2014**, *14*, 5979–5983.
- (10) (a) Pan, Y.; Yuan, B.; Li, Y.; He, D. *Chem. Commun.* **2010**, *46*, 2280–2282. (b) Arnanz, A.; Pintado-Sierra, M.; Corma, A.; Iglesias, M.; Sanchez, F. *Adv. Synth. Catal.* **2012**, *354*, 1347–1355. (c) Cirujano, F. G.; Leyva-Pérez, A.; Corma, A.; iXamena, F. X. L. *ChemCatChem.* **2013**, *5*, 538–549. (d) Li, X.; Guo, Z.; Xiao, C.; Goh, T. W.; Tesfagaber, D.; Huang, W. *ACS Catal.* **2014**, *4*, 3490–3497. (e) Zhao, M.; Deng, K.; He, L.; Liu, Y.; Li, G.; Zhao, H.; Tang, Z. *J. Am. Chem. Soc.* **2014**, *136*, 1738–1741.
- (11) (a) Jiang, H.-L.; Akita, T.; Ishida, T.; Haruta, M.; Xu, Q. *J. Am. Chem. Soc.* **2011**, *133*, 1304–1306. (b) Hermannsdörfer, J.; Friedrich, M.; Miyajima, N.; Albuquerque, R. Q.; Kümmel, S.; Kempe, R. *Angew. Chem., Int. Ed.* **2012**, *51*, 11473–11477. (c) Vilhelmsen, L. B.; Walton, K. S.; Sholl, D. S. *J. Am. Chem. Soc.* **2012**, *134*, 12807–12816. (d) Long, J.; Liu, H.; Wu, S.; Liao, S.; Li, Y. *ACS Catal.* **2013**, *3*, 647–654. (e) Zhu, Q.-L.; Li, J.; Xu, Q. *J. Am. Chem. Soc.* **2013**, *135*, 10210–10213. (f) Chen, Y.-Z.; Xu, Q.; Yu, S.-H.; Jiang, H.-L. *Small* **2015**, *11*, 71–76. (g) Liu, H.; Chen, G.; Jiang, H.; Li, Y.; Luque, R. *ChemSusChem* **2012**, *5*, 1892–1896.
- (12) Férey, G.; Mellot-Draznieks, C.; Serre, C.; Millange, F.; Dutour, J.; Surblé, S.; Margiolaki, I. *Science* **2005**, *309*, 2040–2042.
- (13) (a) Pan, W. T.; Miao, H. Q.; Xu, Y. J.; Navarro, E. C.; Tonra, J. R.; Corcoran, E.; Lahiji, A.; Kussie, P.; Kiselyov, A. S.; Wong, W. C.; Liu, H. *Bioorg. Med. Chem. Lett.* **2006**, *16*, 409. (b) Ayhan-Klcgil, G.; Altanlar, N. *Farmaco* **2003**, *58*, 1345–1350.
- (14) (a) Bellina, F.; Calandri, C.; Cauteruccio, S.; Rossi, R. *Tetrahedron* **2007**, *63*, 1970–1980. (b) Fang, X.; Liu, Z.; Hsieh, M.-F.; Chen, M.; Liu, P.; Chen, C.; Zheng, N. *ACS Nano* **2012**, *6*, 4434–4444.
- (15) Chen, Y.; Wang, H.; Liu, C.-J.; Zeng, Z.; Zhang, H.; Zhou, C.; Jia, X.; Yang, Y. *J. Catal.* **2012**, *289*, 105–117.
- (16) (a) Kim, M.-J.; N, H.-J.; Lee, K. C.; Yoo, E. A.; Lee, M. J. *Mater. Chem.* **2003**, *13*, 1789–1792. (b) Huang, Y.; Lin, Z.; Cao, R. *Chem. Eur. J.* **2011**, *17*, 12706–12712. (c) Sengar, S. K.; Mehta, B. R.; Kulriya, P. K. *J. Appl. Phys.* **2014**, *115*, 124301–124308.
- (17) Huang, X.; Wang, X.; Wang, X.; Wang, X.; Tan, M.; Ding, W.; Lu, X. *J. Catal.* **2013**, *301*, 217–226.